International Journal of Production Research

Publication details, including instructions for authors and subscription information:
http://www.tandfonline.com/loi/tprs20

Directional textures auto-inspection using discrete cosine transform

Der-Baau Perng [a] & Ssu-Han Chen [a]

[a] Department of Industrial Engineering and Management , National Chiao Tung University , HsinChu, Taiwan 30010

Published online: 10 Mar 2011.

To cite this article: Der-Baau Perng & Ssu-Han Chen (2011) Directional textures auto-inspection using discrete cosine transform, International Journal of Production Research, 49:23, 7171-7187, DOI: 10.1080/00207543.2010.495087

To link to this article: http://dx.doi.org/10.1080/00207543.2010.495087

International Journal of Production Research
Vol. 49, No. 23, 1 December 2011, 7171–7187

Taylor & Francis
Taylor & Francis Group

Directional textures auto-inspection using discrete cosine transform

Der-Baau Perng* and Ssu-Han Chen

Department of Industrial Engineering and Management, National Chiao Tung University, HsinChu, Taiwan 30010

(*Received 28 September 2009; final version received 18 May 2010*)

This paper describes a global image restoration scheme using a discrete cosine transform (DCT) that can be used to detect defects in directional textured surfaces automatically. The input spatial domain image is first transformed into the DCT domain so that the dominant directions of the texture in the input image will be compacted into the orthogonal straight lines or impulses through the direct current (DC) component of the spectrum. The linear primitives associated with the high-energies in the DCT domain are eliminated by reducing them to zero before transforming back to the spatial domain. Finally, the defects, if any, are extracted by the thresholding method. Experiments on a variety of product surfaces with directional textures such as straight, slanted, orthogonal, slanted orthogonal, and oblique linear primitives were conducted in this paper. The proposed scheme would blur directional textures and preserved only local defects if they were initially embedded in the image. Furthermore, some preliminary experiments were also conducted to demonstrate the proposed scheme was insensitive to horizontal and vertical shifting, changes in illumination, and image rotation.

Keywords: directional texture; discrete cosine transform; defect inspection; machine vision

1. Introduction

Directional texture in the spatial domain is typically a homogeneous texture that consists of one or more orientation of linear primitives. Directional texture presents almost everywhere in natural and real world images such as woods, straw, fabric textiles, fence, machined surfaces, semiconductor products, etc. Specially, the directionality is an important characteristic which can be easily perceived by the human visual system (Tsai and Hsieh 1999). Non-destructive visual inspection approaches for discriminating textures from abnormalities is quite valuable in industry for assisting with or replacing subjective and repetitive manual inspection processes. Global approaches to inspecting defects in directional textured surfaces usually start with a forward transform and filtering, followed by an inverse transform and thresholding (Kumar 2008). In more detail input image in the spatial domain is first converted to the transform domain where textures exhibit significant high-energy characteristics that can be detected by some pre-defined criteria. After those specific high-energy components have been suppressed in the transform domain, the inverse transform restores the image to the spatial domain. These global approaches thus

*Corresponding author. Email: perng@cc.nctu.edu.tw

ISSN 0020–7543 print/ISSN 1366–588X online

http://dx.doi.org/10.1080/00207543.2010.495087
http://www.tandfonline.com

preserve only the local defects that existed in the original input image, and remove all directional textures.

Possible approaches to detecting surface defects include the use of discrete Fourier transform (DFT) (Tsai and Hsieh 1999, Perng *et al*. 2010), discrete wavelet transform (DWT) (Tsai and Chiang 2003), singular value decomposition (SVD) (Lu and Tsai 2004), principal component analysis (PCA) (Chen and Perng 2011), and independent component analysis (ICA) (Lu and Tsai 2008). State-of-the-art global directional textured surface inspectors can be generally categorised into three types: DFT and DWT, which are regarded as frequency-based methods; SVD and PCA, which are subspace-based methods; and ICA, which is a filter-based method. Each of these methods may be a good choice for implicit or qualitative inspection of directional textured surfaces. Because these methods require neither textural features nor any reference image for comparison, they are immune to the limitations inherent in local feature extraction or golden template matching methods (Lin 2008).

In this paper, a new frequency-based global image restoration scheme using the discrete cosine transform (DCT) for automatic surface quality control is presented. The DCT has excellent energy compaction ability for correlated textures like periodic linear primitives. It converts the input image into the DCT domain and has the property of packing the most information into the fewest coefficients. The first component in the transformed set is the most meaningful; the latter, the least. In particular, the energy of the dominant textures is concentrated in the top-left low-frequency region, whereas the energy of the local defects is spread out only on the relatively high-frequency region. This allows users to discard coefficients with relatively large amplitudes without introducing textures into the restored image. Statistically process control (SPC) binarization is used to set the upper and lower thresholds for discriminating between uniform elements and defective regions in the restored image.

The rest of this paper is organised as follows. In Section 2, the DCT applications to defect inspection is reviewed. In Section 3, the proposed DCT-based image restoration scheme is described. In Section 4, the experimentation and corresponding results are presented. Our concluding remarks are given in Section 5.

2. DCT applications to defect inspection

In automated surface inspection, one has to solve the problem of detecting defects which embedded in an inspected image by means of DCT. Conventionally, a spatial domain image is converted to a DCT domain and some representative features of certain bands of the spectrum are computed. Then the suspected defects can be easily detected by classifiers because the used features usually have distinct values. Tan and Kittler (1992) extracted DCT features from each of the three RGB colour bands for classifying colour textures. Ünsalan and Erçil (1998) used some DCT features of certain bands of DCT for classifying defective wood surfaces or clear ones. Hsu (2007) converted inspected optical component image into DCT domain and features of each DCT block were extracted. Then the defect blocks were determined by the Hotelling T^2 statistic. The disadvantages of the local approach include: (1) hard for selecting a set of optimal textural features for discrimination, (2) failure of completely imitating a set of optimal features of a specific texture to other texture patterns, (3) the time consumed computing the feature values of a very large macro window (Tsai and Chiang 2003, Lin 2008).

On the contrary, in the last decade, many vision systems have been developed for the inspection of surface defects based on DCT-based global restoration strategies. The advantages of the global approach have been addressed in Section 1. He *et al.* (2005) detected small defects on the leather surface. Lin and Ho (2007) inspected tiny pinhole defects in surface barrier layer (SBL) chips. Lin (2008) examined tiny defects on the surfaces of electronic passive components. Chen and Kuo (2008) used DCT for detecting mura defects on thin-film transistor liquid crystal displays (TFT-LCD). All of these used a global image restoration strategy for defect inspection based on the DCT. However, the works of He *et al.* (2005) and Lin and Ho (2007) engaged only with random textures, Lin (2008) concentrated only on single circle-shaped primitives, and Chen and Kuo (2008) studied only images with uniform intensities. Their works did not address the central theme of this paper. That is, the important topic of directional textured surface inspection using the DCT has not yet been examined.

3. DCT-based defect detection

3.1 *Discrete cosine transform*

Several DCT variants have been proposed. These were categorised by Wang (1984) into four slightly different transformations: DCT-I, DCT-II, DCT-III, and DCT-IV. The DCT-II is used in this research because of its ability to process images with uneven boundaries. Equation (1) is the expression for computing the two-dimensional DCT of an $m \times n$ input image $f(x, y)$.

$$C(u,v) = \alpha(u)\alpha(v)\sum_{x=0}^{m-1}\sum_{y=0}^{n-1} f(x,y)\cos\left[\frac{(x,y)u\pi}{2m}\right]\cos\left[\frac{(2y+1)v\pi}{2n}\right] \tag{1}$$

for $u = 0, 1, \ldots, m-1$ and $v = 0, 1, \ldots, n-1$, where $\alpha(u)$ and $\alpha(v)$ are defined as

$$\alpha(u) = \begin{cases} \sqrt{\dfrac{1}{m}}, & u = 0 \\ \sqrt{\dfrac{2}{m}}, & u = 1, 2, \ldots, m-1 \end{cases} \quad \alpha(v) = \begin{cases} \sqrt{\dfrac{1}{n}}, & v = 0 \\ \sqrt{\dfrac{2}{n}}, & v = 1, 2, \ldots, n-1 \end{cases} . \tag{2}$$

In this paper, $C(0, 0)$ is first set equal to zero for reasons explained in Section 4.3. Then the wide dynamic range of $C(u, v)$ for $u \neq 0$ and $v \neq 0$ is mapped into the narrow range of $P(u, v)$ by a logarithmic transformation, and scaled its intensity into an eight-bit gray level using

$$P(u,v) = S\left[\log\left(1 + \left|C(u,v)\right|^2\right)\right] \tag{3}$$

where $S(\cdot)$ is a scaling operation. The origin of the DCT coefficient has a very large energy and so is referred to as the direct current (DC) component of the spectrum, while the other coefficients are the alternating current (AC) components. The DC coefficients in the upper

left corner reflect information with a low frequency, whereas the AC coefficients in the lower right corner reflect progressively higher frequencies (Gonzalez and Woods 2008). The DCT has the property of packing the dominant energy of a given image into the low-frequency region. In particular, when the textures of an image are composed of linear primitives, the dominant directions (the orientation of the main pattern inside a given image which is easily recognised by the human perception) will be compacted as corresponding orthogonal straight lines or impulses throughout the DC component in the spectrum. In other words, lines in the spatial domain and their transformed counterparts in the DCT domain are orthogonal to each other.

As shown in Figures 1(a1)–1(a5), five artificial images containing straight, slanted, orthogonal, slanted orthogonal, and oblique linear structures were used to demonstrate

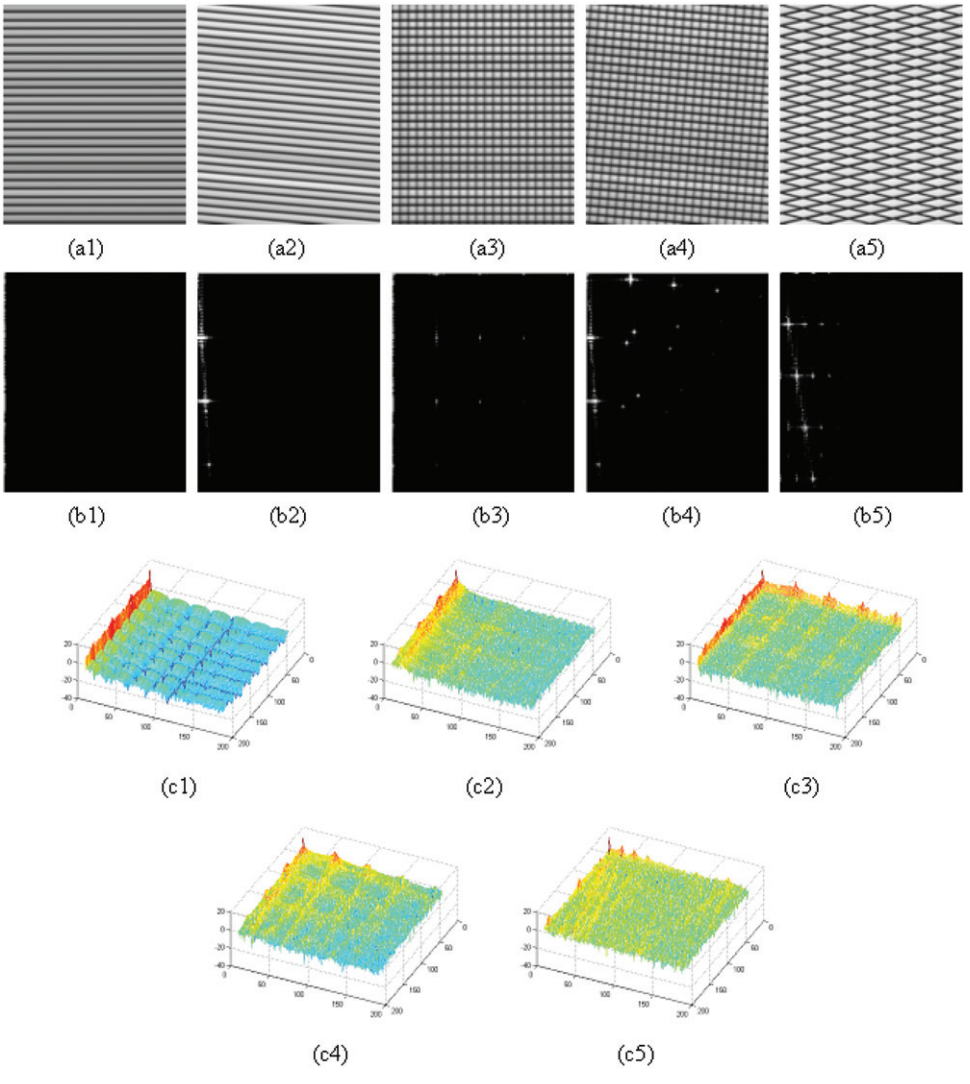

Figure 1. (a1)–(a5) Artificial images with different linear primitives, (b1)–(b5) corresponding spectra, and (c1)–(c5) corresponding 3D energy plots.

the DCT compaction capability for well-defined linear primitives. The forward DCT to these images was applied and the spectra shown in Figures 1(b1)–1(b5), respectively was obtained; Figures 1(c1)–1(c5) showed the corresponding three-dimensional (3D) energy plots. The dominant directions in Figures 1(a1)–1(a5) were compacted to orthogonal straight lines or impulses through the DC component, as shown in the corresponding Figures 1(b1)–1(b5). In addition, Figures 1(c1)–1(c5) clearly showed that the high-energy components were packed around the top left regions. These are all inherent characteristics of the DCT basis function.

3.2 *DCT-based image restoration*

The linear primitives in the spatial domain are highly concentrated in the high-energy components distributed along the transformed lines or impulses in the DCT domain. These coefficients can be edited in advance in the surface defect inspection application, usually ignoring the high-energy components and retaining the rest to restore the image with the inverse discrete cosine transform (IDCT) for background texture removal. More specifically, $C_T(u, v)$ is defined to be the modified coefficients in Equation (4). This means that after the DCT operation, only the frequency components whose powers are greater than or equal to the high-energy threshold T are discarded. In other words, some high-energy components in the spectrum image can be selected based on the value of T, and be set to zero.

$$C_T(u, v) = \begin{cases} 0, & \text{if } P(u, v) \geq T \\ C(u, v), & \text{otherwise} \end{cases} \tag{4}$$

where $T \in [1, 255]$. After checking the coefficients in the DCT domain using Equation (4), the image can be restored using the IDCT,

$$\hat{f}(x, y) = \sum_{u=0}^{m-1} \sum_{v=0}^{n-1} \alpha(u)\alpha(v) C_T(u, v) \cos\left[\frac{(2x+1)u\pi}{2m}\right] \cos\left[\frac{(2y+1)v\pi}{2n}\right] \tag{5}$$

for $x = 0, 1 \ldots, m-1$ and $y = 0, 1, \ldots, n-1$, where $\alpha(u)$ and $\alpha(v)$ are defined in Equation (2).

An artificial image was used to demonstrate the defect-preserving ability of the DCT-based image restoration scheme. Figure 2(a) was an image derived from Figure 1(a2) with some spot defects on it. Figure 2(a) was transformed into the DCT space; Figures 2(b)

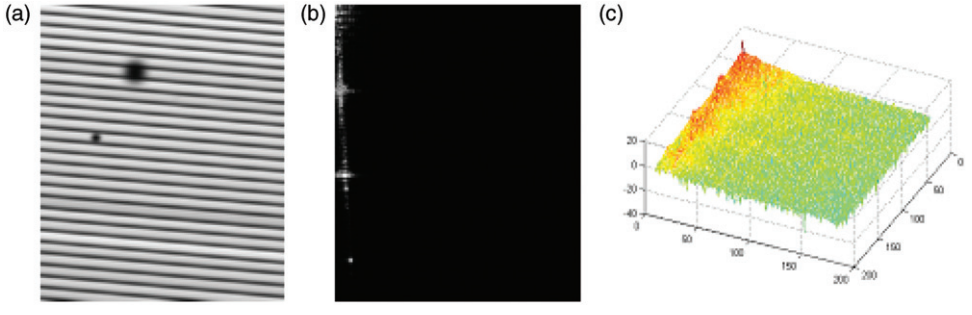

Figure 2. (a) Image of Figure 1(a2) with artificial spot defects, (b) corresponding spectrum, and (c) corresponding 3D energy plot.

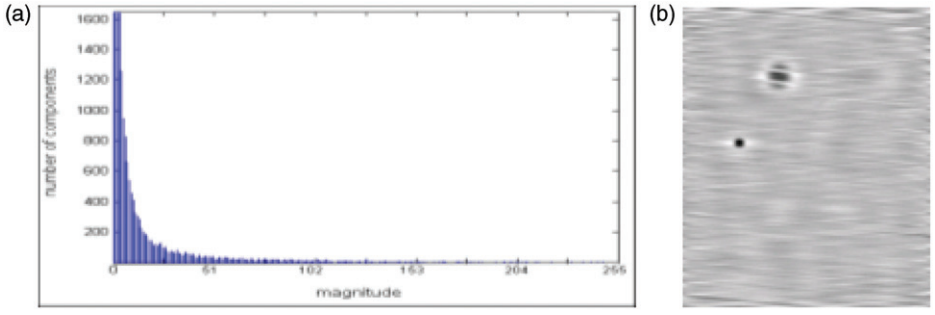

Figure 3. (a) Power distribution of Figure 2(a) and (b) restored images when T was selected using the Rosin thresholding method.

and 2(c) showed the resulting energy plots. The lines in Figures 2(b)–2(c) were less compact (more dispersed) than those in Figures 1(b2)–1(c2) because the regularity of the directional textures was interrupted by the spot defects.

Here the issue of how to determine the threshold value T is described. In general, the larger coefficients in Equation (1) come from the transformation of background textures, whereas the remaining coefficients with zero or near-zero magnitude are the result of other detailed information or defects in the input image. Stacking the DCT coefficient powers produces an exponential histogram, as shown in McLaren and Nguyen (1991). Rosin thresholding was used in this method to determine a threshold value in such a unimodal histogram for separating textures from the remaining information (Rosin 2001). Rosin thresholding automatically determines a corner of the exponential histogram and the response of the corresponding power magnitude, i.e., T. It modifies the DCT coefficients in Equation (4) and removes the directional textures while retaining the defects in the images restored using Equation (5). Figure 3(a) showed the stacked powers of Figure 2(a) with an exponential shape. Figure 3(b) gave the restored result based on the value of T, which was determined by using the Rosin thresholding method. The global texture in Figure 3(b) was well removed or blurred while the local dark spot defects were distinctly preserved. Section 4.1 gives more experimental results related to inspecting defects in real-world directional textured images to demonstrate the robustness of this scheme.

3.3 *Statistical process control binarization*

Because the intensities of the pixels in the restored image varied only slightly, the statistical process control (SPC) binarization method is used to establish the upper and lower control limits for highlighting the defects. The SPC binarization method is

$$\tilde{f}(x,y) = \begin{cases} 255 & \text{if } \mu - c\cdot\sigma < \tilde{f}(x,y) < \mu + c\cdot\sigma \\ 0 & \text{otherwise} \end{cases} \tag{6}$$

where c is a control constant, and μ and σ are the mean and standard deviation, respectively, of the gray levels in the restored image. If a pixel has a gray level that falls between the upper and the lower limits, it is shown as white and is considered to be a texture element to be removed. Otherwise, it is shown as black and is considered to be a defective element to be preserved. Figure 4 shows the binarized result of Figure 3(b) for

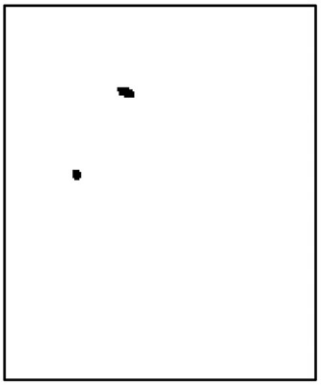

Figure 4. Binarized version of Figure 3(b) with $c = 5$.

$c = 5$, which clearly produced white directional textures and dark defects. Blob analysis can always be used to remove the small-area noise blobs. The threshold for small-area noise blobs can be set in terms of the requirement specification.

4. Experimental results

The proposed DCT-based image restoration scheme was implemented to evaluate its performance in detecting defects on the surfaces of several different products. Several types of directional texture patterns with defective or defect-free samples were used, including images of an organic light-emitting diode (OLED), internal thread, polymer light-emitting diode (PLED), contact lens dioptric pattern, and diamond mesh. Some preliminary experiments were also conducted to demonstrate the effects of the proposed scheme in the presence of horizontal or vertical shifting, illumination changes, and image rotation.

4.1 *Directional texture surface inspection*

Parameter c of the proposed scheme should initially be selected in a pre-training stage. Fifteen individual training samples (seven defect-free and eight defective samples) were prepared. The number of correct detections was recorded in a supervised manner for values of c in the range 0.5–8.0 at increments of 0.5, and the value of c that resulted in the highest correct detection rate was selected. The c values for the SPC formula values of 5.5, 6.5, 6.0, 4.5, and 5.0 were selected for the five products.

After the initial c-training stages, some images for follow-up defect inspection were tested. Figures 5(a1)–5(a4) to 9(a1)–9(a4) show one defect-free and three defective product surfaces with distinct defects. Figures 5(b1)–5(b4) to 9(b1)–9(b4) show the corresponding restored images using the DCT-based image restoration scheme. Note that the directional textures of these product surfaces were almost eliminated. Figures 5(c1)–5(c4) to 9(c1)–9(c4) show the corresponding binarized images generated by SPC binarization with $c = 5.5$, 6.5, 6.0, 4.5, and 5.0, respectively. Note that Figures 5(c1)–5(c1) shows clear responses, and Figures 5(c2)–5(c4) to 9(c2)–9(c4) show the defects that were initially embedded in the product surfaces.

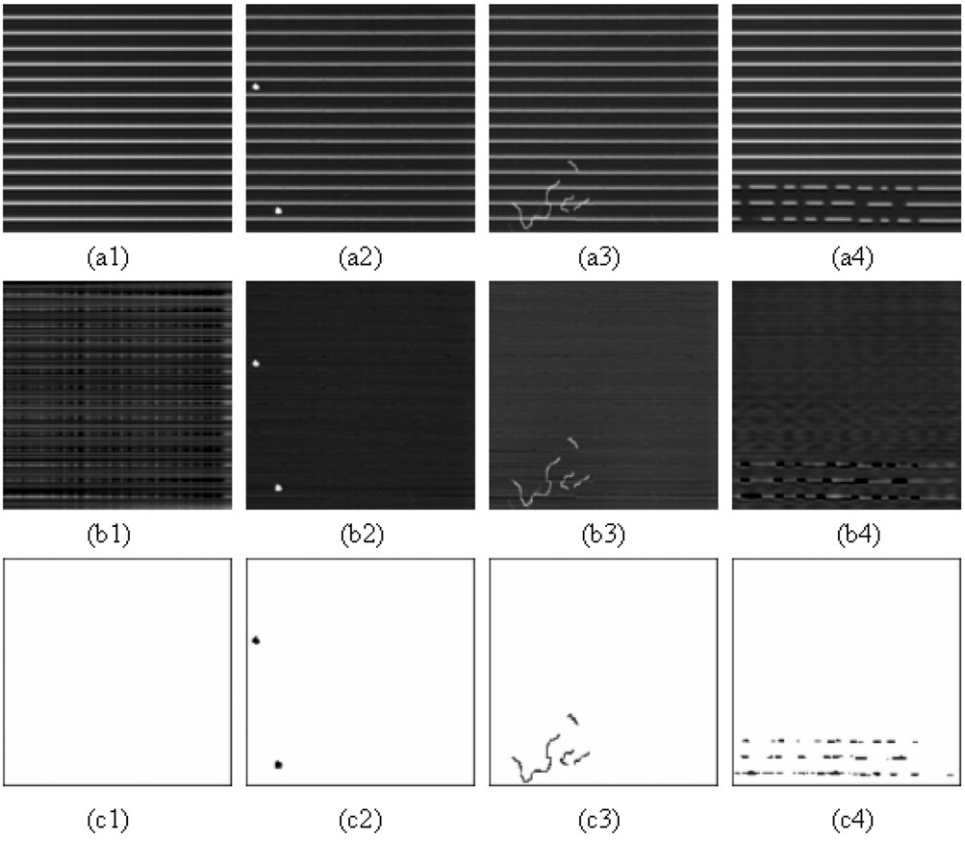

Figure 5. (a1)–(a4) One defect-free OLED panel and three defective ones with a hole, a scratch, and an erosion; (b1)–(b4) corresponding restored images; and (c1)–(c4) corresponding binarized images.

The proposed scheme indicated the defect location and roughly preserved the defect shape. In real-world applications, the defect location can be used not only for backtracking or reference, but also to analyse the type of defect distribution (e.g., random or clustered) on the surface for in-process monitoring and control. The defect shape can provide extra geometrical features (e.g., area, elongation, centroid, or perimeter) by blob analysis to identify the defect compared to the specification, or for recognising the defect type by providing discriminating features to a classifier.

4.2 *Effect of image shifting*

The effect of the proposed DCT-based image restoration scheme in the presence of shifting was evaluated. Samples for this experiment were taken from Figures 7(a1) and 7(a2). Because the PLED sample consisted of a 10×10-pixel rectangular pattern, only the 1-, 3-, 5-, 7-, and 9-pixel vertically or horizontally shifted versions shown in Figures 10(a1)–10(a10) and Figures 11(a1)–11(a10), respectively, were tested using the fixed parameter $c = 6.0$. The proposed scheme produced clear results and highlighted defects on the

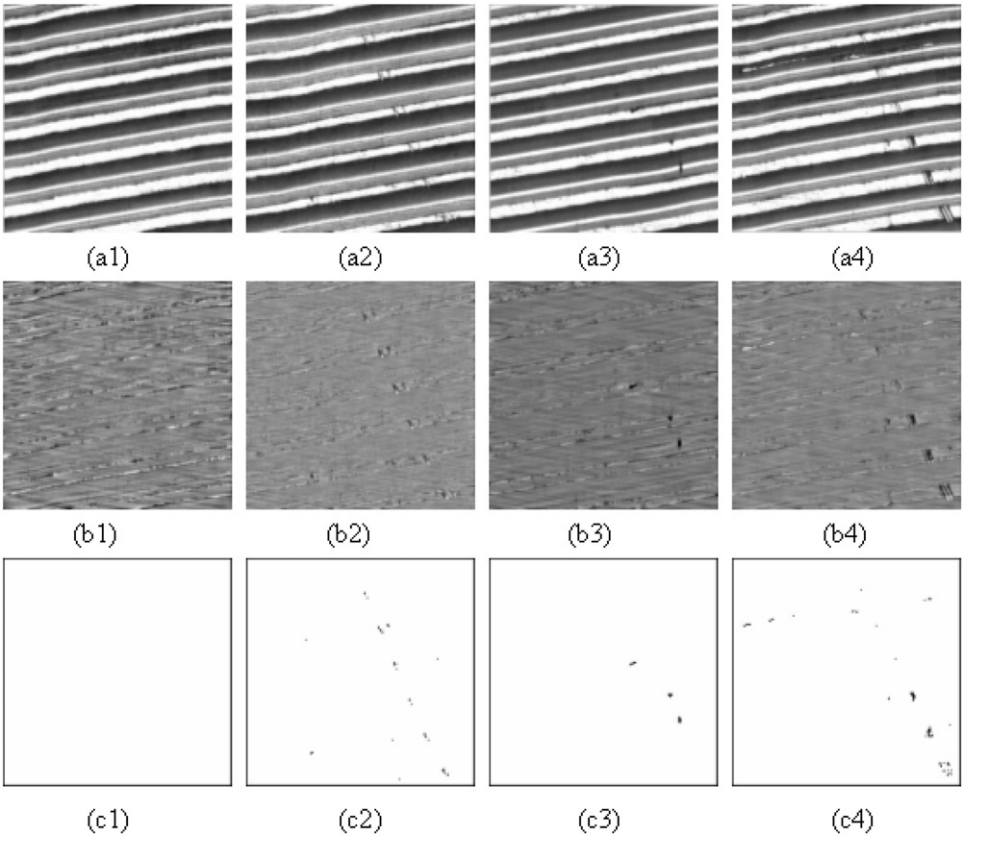

Figure 6. (a1)–(a4) One defect-free internal thread and three defective ones with a collapse, a collapse/flaw, and a collapse/scratch; (b1)–(b4) corresponding restored images; and (c1)–(c4) corresponding binarized images.

surfaces even when the spatial arrangement had been changed, as shown in Figures 10(b1)–10(b10) and Figures 11(b1)–11(b10)

Because of the ''shift in time'' property of the DCT discussed in Sherlock and Kakad (2001), the DCT coefficients of the original image were different than those of the shifted images. However, for directional textured images, Figures 10(a1)–10(a10) and 11(a1)–11(a10), noted that the histogram of the DCT coefficients had similar distributions, as shown in Figures 12(a) and 12(b). The Rosin thresholding method thus adaptively generated a proper high-energy threshold in Equation (4). Furthermore, note that the individual directional textures of Figures 5(a1)–5(a4) to Figures 9(a1)–9(a4) were not completely identical; there was slight horizontal or vertical shifting. Even so, the proposed scheme still provided correct responses independent of the amount of shifting. Thus, the proposed scheme was able to detect defects in directional textured images and was invariant to horizontal or vertical shifting of the directional texture. This shift-invariance property is quite useful for inspecting large object surfaces in real-world applications. Users could arrange several cameras in an automated optical inspection (AOI) system in parallel across the inspected object. These cameras could be moved to the next portion to

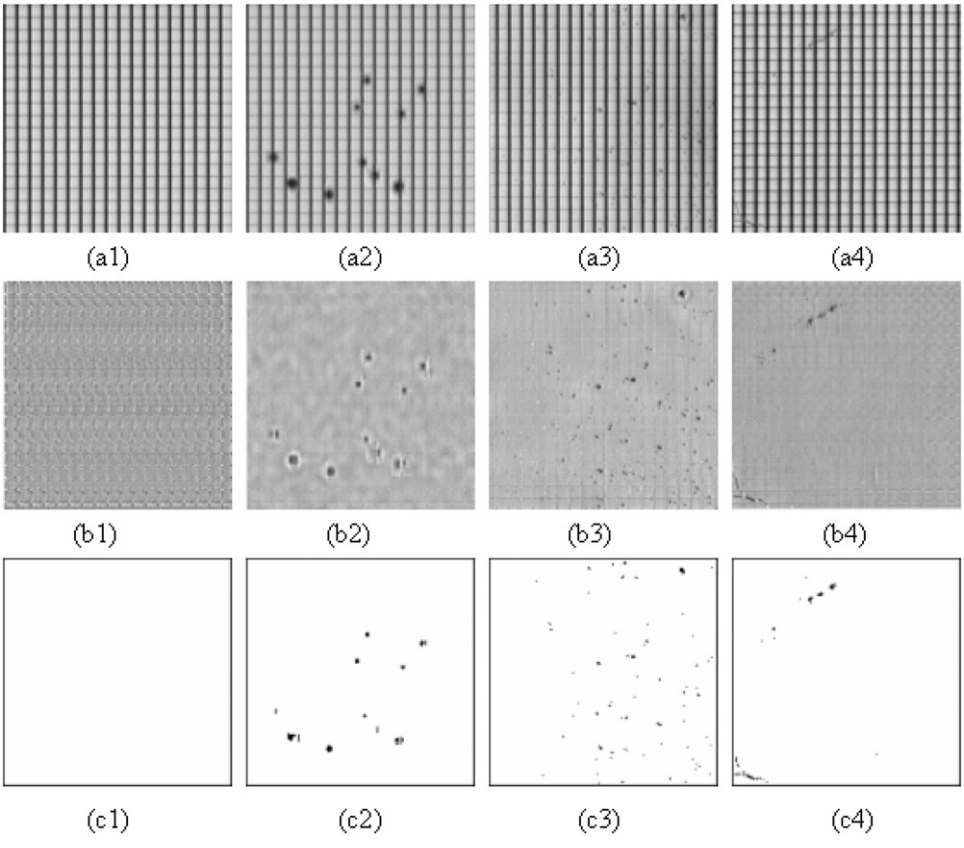

Figure 7. (a1)–(a4) One defect-free PLED panel and three defective ones with a dark point, a particle, and a scratch; (b1)–(b4) corresponding restored images; and (c1)–(c4) corresponding binarized images.

continue the inspection process. In general, the textures in each sub-image scanned with different fields of view may not appear in exactly the same manner and may be accompanied by slight shifting. The shift-invariance property of the proposed scheme handles this complex case and is useful for inspecting sub-images of large objects. Moreover, the shifting caused by errors in machine actuators can also be generally tolerated.

4.3 *Effect of change in illumination*

The effect of the proposed DCT-based image restoration scheme under conditions of varying illumination was evaluated. Using a uniform light source system, subtractive and additive illumination changes were applied to Figures 7(a1) and 7(a2), respectively, to simulate the underexposed and overexposed conditions shown in Figures 13(a1), 13(a2) and Figures 13(a3), 13(a4). The proposed scheme to the images was applied using the fixed parameter $c = 6.0$. As shown in Figures 13(b1)–13(b4), the proposed scheme produced clear results and highlighted the defects on the surfaces under all illumination conditions.

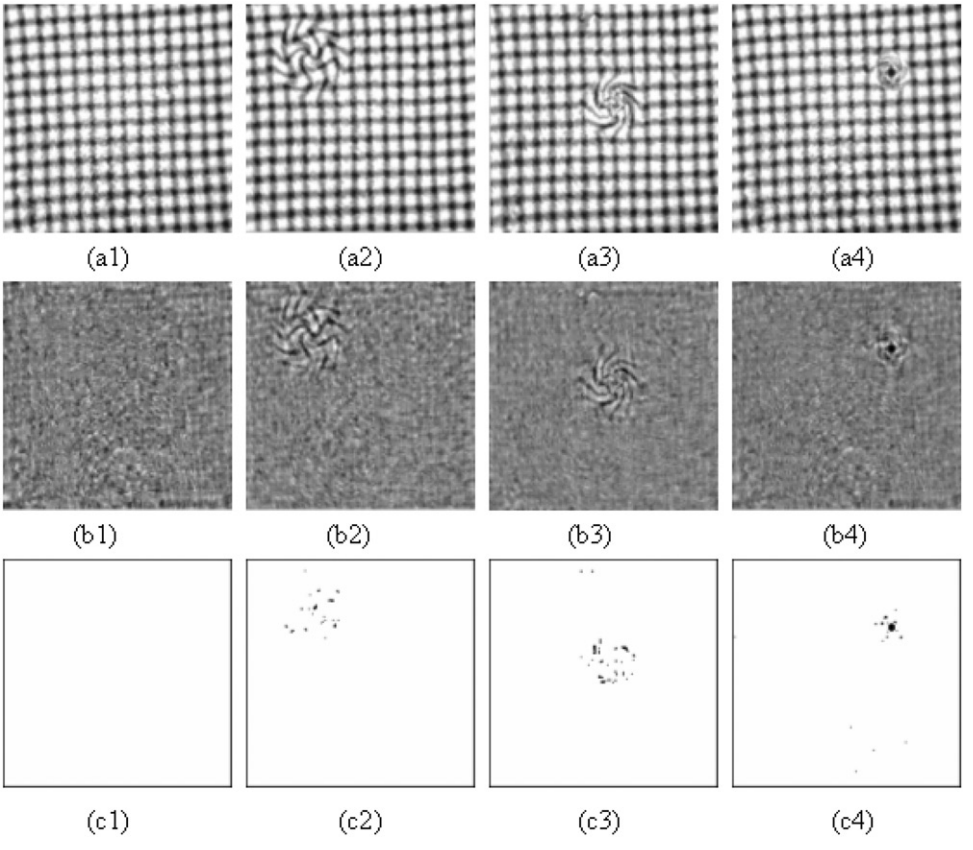

Figure 8. (a1)–(a4) One defect-free contact lens dioptric pattern and three defective ones with a twist, an eddy, and a dark point; (b1)–(b4) corresponding restored images; and (c1)–(c4) corresponding binarized images.

Because the DCT-II is a linear and distributive unitary transform (Lukac and Plataniotis 2006), the illumination change will affect the DC component, i.e., the average gray level of an image, only. Since the proposed scheme reduces the DC component to zero before the scaling operation of Equation (3), a change in illumination will affect neither the distribution of the remaining AC components nor the determination of the high-energy threshold. Therefore, as long as the textures and defects of an image are clear enough (i.e., not distorted), the proposed scheme is robust to varying illumination conditions. This illumination-invariance property of the proposed scheme will reduce the rate of false alarms or missed detections if the AOI system encounters unexpected uniform light source instability in real-world applications.

4.4 *Effect of image rotation*

The effect of the proposed DCT-based image restoration scheme in the presence of image rotations was evaluated. Figures 14(a1)–14(a5) and 15(a1)–15(a5) were obtained by rotating Figures 7(a1) and 7(a2) by 9°, 18°, 27°, 36°, and 45°, respectively. Then the

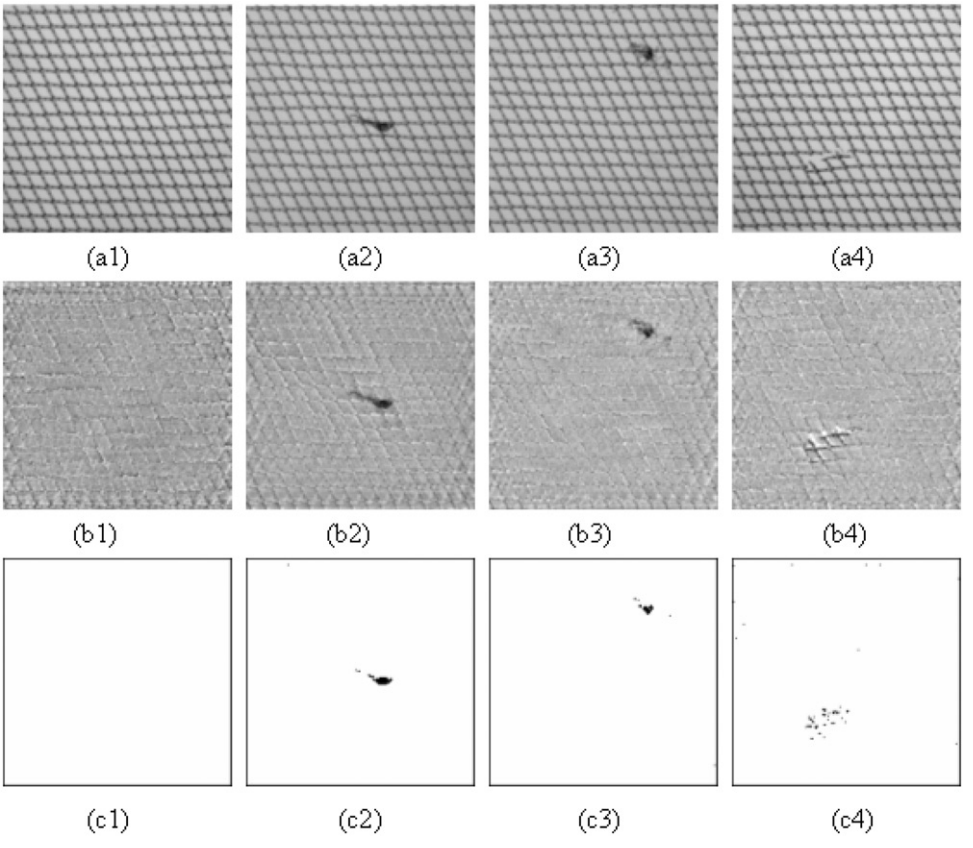

Figure 9. (a1)–(a4) One defect-free diamond mesh and three defective ones with a particle, a fiber, and a cut; (b1)–(b4) corresponding restored images; and (c1)–(c4) corresponding binarized images.

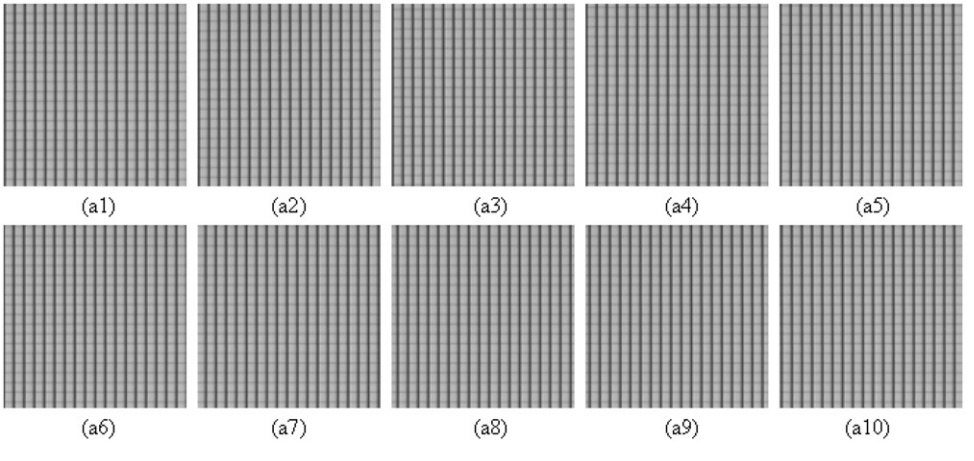

Figure 10. (a1)–(a5) and (a6)–(a10) are the same as Figure 7(a1) shifted vertically and horizontally by 1, 3, 5, 7, and 9 pixel(s), respectively; (b1)–(b5) and (b6)–(b10) are the corresponding binarized images.

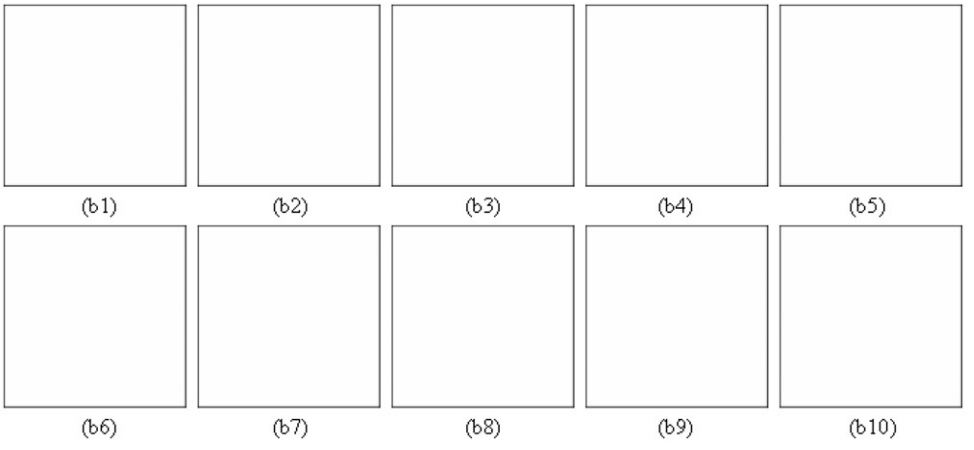

Figure 10. Continued.

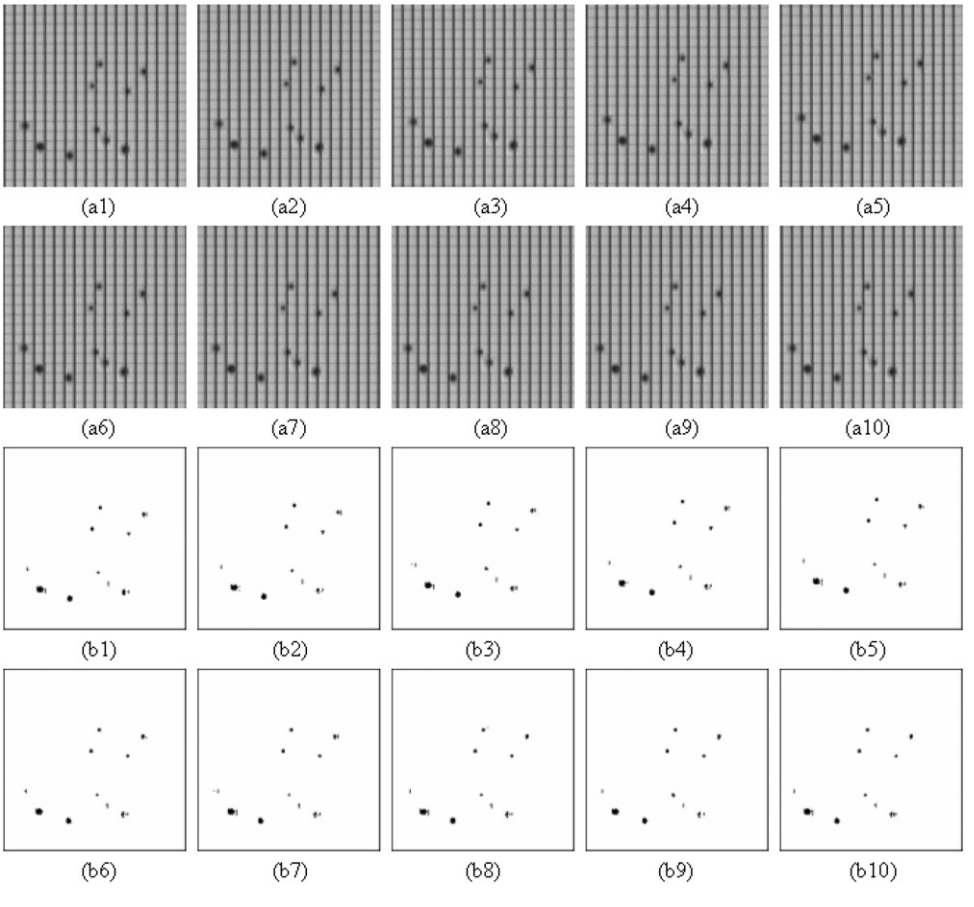

Figure 11. (a1)–(a5) and (a6)–(a10) are the same as Figure 7(a2) shifted vertically and horizontally by 1, 3, 5, 7, and 9 pixel(s), respectively; (b1)–(b5) and (b6)–(b10) are the corresponding binarized images.

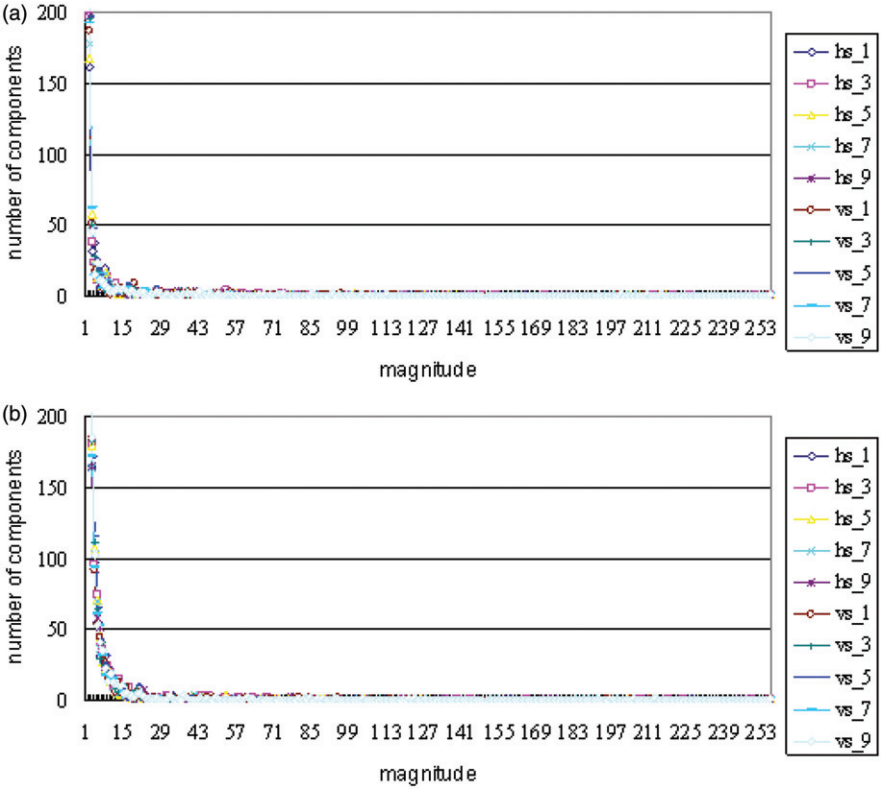

Figure 12. (a) and (b) are the histograms of the DCT coefficients of Figures 10(a1)–10(a10) and Figures 11(a1)–11(a10), respectively. The case of zero magnitude was neglected due to its huge number of components. The notations "hs_#" and "vs_#" indicate the amount of horizontal or vertical shift in pixel(s).

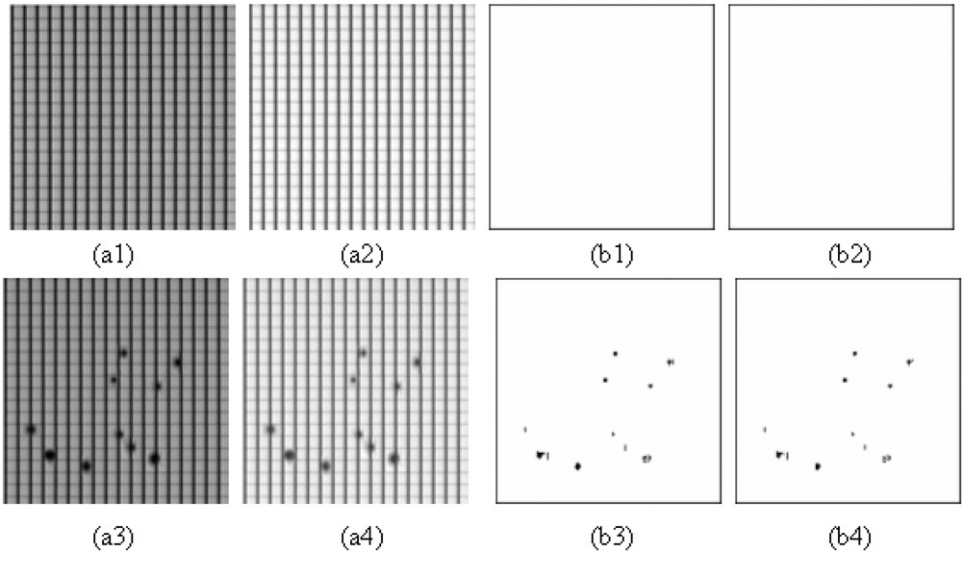

Figure 13. (a1)–(a4) are derived by changing the illumination of Figures 7(a1) and 7(a2); (b1)–(b4) are the results of binarizing (a1)–(a4).

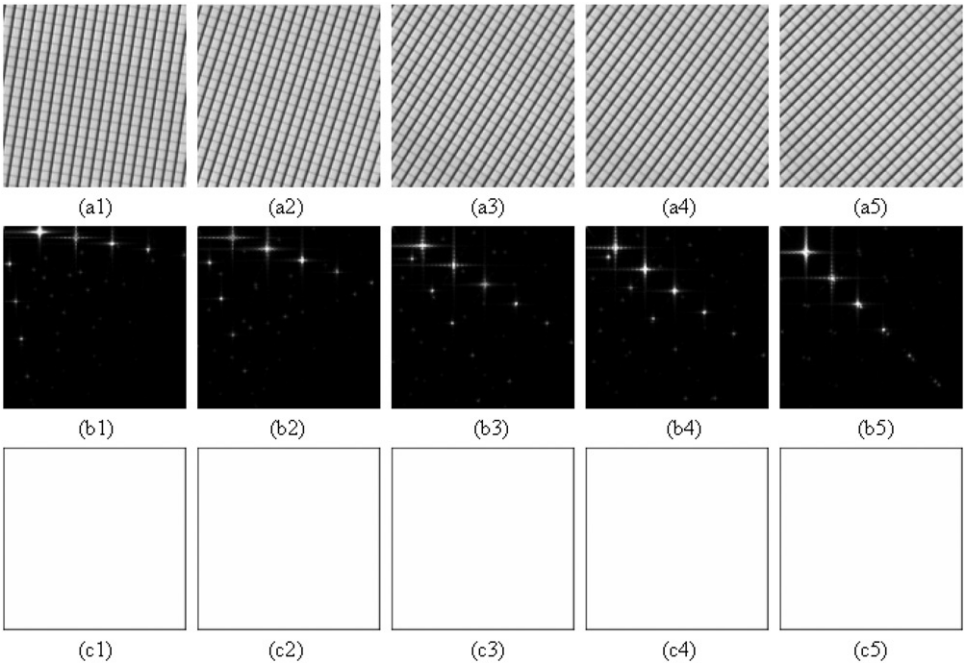

Figure 14. (a1)–(a5) are obtained by rotating Figure 7(a1) by 9°, 18°, 27°, 36°, and 45°, respectively; (b1)–(b5) are the corresponding spectra of (a1)–(a5), respectively; and (c1)–(c5) are the binarized versions of (b1)–(b5), respectively.

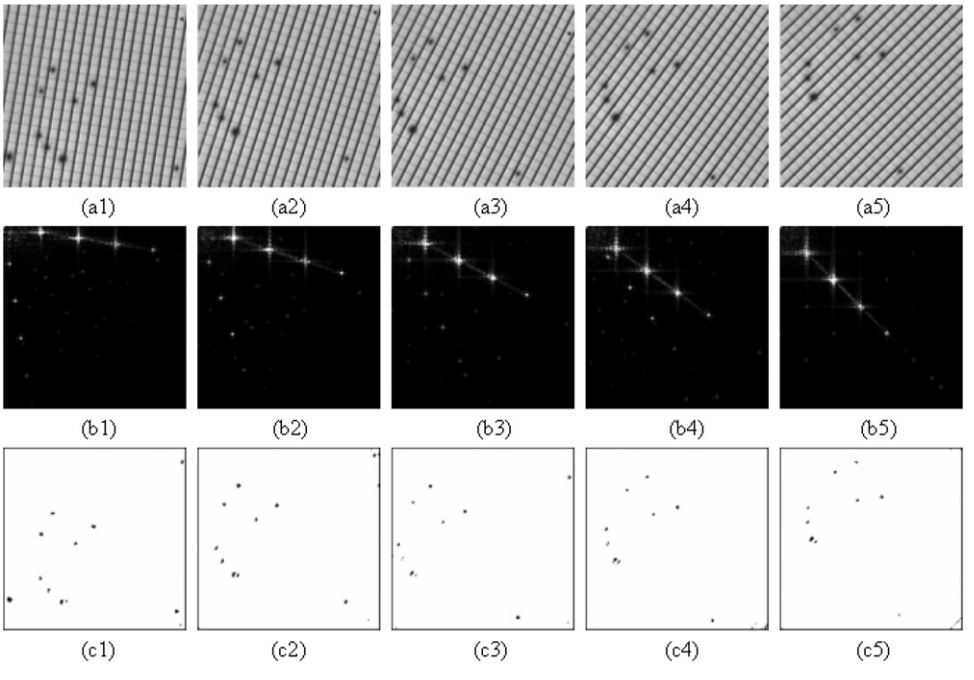

Figure 15. (a1)–(a5) are derived by rotating Figure 7(a2) by 9°, 18°, 27°, 36°, and 45°, respectively; (b1)–(b5) are the corresponding spectra of (a1)–(a5), respectively; and (c1)–(c5) are the binarized version of (b1)–(b5), respectively.

proposed scheme to the images was applied using the fixed parameter $c = 6.0$. The distribution of the high-energy components in Figures 14(b1)–14(b5) and Figures 15(b1)–15(b5) rotated gradually following the directional textures in Figures 14(a1)–14(a5) and Figures 15(a1)–15(a5), remaining orthogonal. After suppressing the high-energy components related to the texture and binarizing the restored image, it is clear that the proposed scheme produced good results and highlighted defects on the surfaces, even when the images had been rotated, as shown in Figures 14(c1)–14(c5) and Figures 15(c1)–15(c5). The results of Figures 14 and 15 thus show that the proposed scheme is insensitive to image rotation. This rotation-invariance will eliminate tedious calibrations in real-world applications because they will require neither an extremely precise AOI hardware fixture for object placement nor an effective AOI software algorithm for image reversal.

5. Conclusions

A new global DCT-based image restoration scheme for detecting defects in directional textured surfaces is described in this paper. The scheme first transforms the input image into the DCT domain. Linear primitives associated with high-energy components in the DCT domain are determined by the Rosin thresholding method and then reduced to zero. After the suppressed DCT image is transformed back to the spatial domain and binarized by SPC binarization, the textures are removed in the final image while any original defects are distinctly preserved. A defect-free directional texture surface image resulted in a clear response in our experiments; otherwise, distinct defects were clearly identified by rough shapes in precise locations. This demonstrated the ability of the proposed scheme to detect defects on surfaces with various periodic linear patterns. The proposed global DCT-based restoration scheme was insensitive to horizontal and vertical shifting, changes in illumination, and image rotation. These three characteristics greatly enhance the practicality of the proposed scheme for industrial inspection. Furthermore, in comparison with existing global approaches that mentioned in Section 1, DFT is a complex transform with lower computational efficiency than DCT which is a real transform (Rao and Yip 1990). Because DWT depends on the length of the wavelet filters, the complexity of DWT is higher than that of DCT (Feig 1990, Xiong *et al*. 1999). Besides, the complexity of both SVD and PCA is significantly higher than that of DCT, due to the derivation of the respective basis for each image (Khayam 2003). Finally, ICA is an iterative and learning algorithm, so it requires a great deal of computational resources. It is well acknowledged that hardware or software implementation of the DCT is less cost expensive than that of existing global methods.

The scheme proposed in this paper focuses on directional textures. Inspecting defects in statistical textures remains a subject for further investigation.

Acknowledgements

This research is partially supported by the National Science Council, Taiwan, under contract No. NSC 97-2221-E-009-112-MY3.

References

Chen, L.C. and Kuo, C.C., 2008. Automatic TFT-LCD mura defect inspection using discrete cosine transform-based background filtering and 'just noticeable difference' quantification strategies. *Measurement Science and Technology*, 19 (1), 015507.

Chen, S.H. and Perng, D.B., 2011. Directional textures auto-inspection using principal component analysis. *The International Journal of Advanced Manufacturing*, DOI: 1007/500170-010-3141-1.

Feig, E., 1990. A fast scaled DCT algorithm. *Proceedings of SPIE*, Santa Clara, CA, USA, 1244 (2), 2–13.

Gonzalez, R.C. and Woods, R.E., 2008. *Digital image processing*. Upper Saddle River, NJ: Pearson/Prentice Hall.

He, F., Wang, W., and Chen, Z., 2005. Detection of small surface defects using DCT based enhancement approach in machine vision systems. *Proceedings of SPIE*, 6040.

Hsu, S.Y., 2007. *Applying block discrete cosine transform and grey clustering algorithm to automated visual defect inspection of optical components*. Thesis (Master). Chaoyang University of Technology.

Khayam, S.A., 2003. *The discrete cosine transform (DCT): theory and application* [online]. Seminar Note, Michigan State University. Available from: http://www.egr.msu.edu/waves/people/Ali_files/DCT_ TR802.pdf [Accessed 10 January 2010].

Kumar, A., 2008. Computer-vision-based fabric defect detection: a survey. *IEEE Transactions on Industrial Electronics*, 55 (1), 348–363.

Lin, H.D., 2008. Tiny surface defect inspection of electronic passive components using discrete cosine transform decomposition and cumulative sum techniques. *Image and Vision Computing*, 26 (5), 603–621.

Lin, H.D. and Ho, D.C., 2007. Detection of pinhole defects on chips and wafers using DCT enhancement in computer vision systems. *International Journal of Advanced Manufacturing Technology*, 34 (5–6), 567–583.

Lu, C.J. and Tsai, D.M., 2004. Defect inspection of patterned thin film transistor-liquid crystal display panels using a fast sub-image based SVD. *International Journal of Production Research*, 42 (20), 4331–4351.

Lu, C.J. and Tsai, D.M., 2008. Independent component analysis-based defect detection in patterned liquid crystal display surfaces. *Image and Vision Computing*, 26 (7), 955–970.

Lukac, R. and Plataniotis, N.K., 2006. *Color image processing: methods and applications*. Boca Raton: FL: CRC Press/Taylor & Francis.

McLaren, D.L. and Nguyen, D.T., 1991. Removal of subjective redundancy from DCT-coded images. *IEE Proceedings I Communications, Speech and Vision*, 138 (5), 345–350.

Perng, D.B., Chen, S.H., and Chang, Y.S., 2010. A novel internal thread defect auto-inspection system. *The International Journal of Advanced Manufacturing*, 47 (5–8), 731–743.

Rao, K.R. and Yip, P., 1990. *Discrete cosine transform: algorithms, advantages, applications*. San Diego, CA: Academic Press Professional, Inc.

Rosin, P.L., 2001. Unimodal thresholding. *Pattern Recognition*, 34 (11), 2083–2096.

Sherlock, B.G. and Kakad, Y.P., 2001. Windowed discrete cosine and sine transforms for shifting data. *Signal Processing*, 81 (7), 1465–1478.

Tan, S.C. and Kittler, J., 1992. On colour texture representation and classification. *2nd International Conference on Image Processing*, 390–395.

Tsai, D.M. and Chiang, C.H., 2003. Automatic band selection for wavelet reconstruction in the application of defect detection. *Image and Vision Computing*, 21 (5), 413–431.

Tsai, D.M. and Hsieh, C.Y., 1999. Automated surface inspection for directional textures. *Image and Vision Computing*, 18 (1), 49–62.

Ünsalan, C. and Erçil, A., 1998. *Defect inspection of wood surfaces* [online]. Bogaziçi University Research Report, FBE-IE-08/97-12. Available from: http://vision.yeditepe.edu.tr/files/tr1.pdf [Accessed 10 January 2010].

Wang, Z., 1984. Fast algorithms for the discrete W transform and for the discrete Fourier transform. *IEEE Transactions on Acoustics, Speech, and Signal Processing*, 32 (2), 803–816.

Xiong, Z., *et al*., 1999. A Comparative study of DCT- and wavelet-based image coding. *IEEE Transactions on Circuits and Systems for Video Technology*, 9 (5), 692–695.